2026 Volume: 02 Issue: 08 www.ijrpa.com ISSN 2456-9995 Research Article

International Journal Research Publication Analysis

Page: 01-26

ANALYSIS OF CATTANEO–CHRISTOV HEAT FLUX AND RADIATIVE EFFECTS ON TRI-HYBRID NANOFLUID FLOW IN MAXWELL AND CROSS FLUIDS WITH APPLICATION TO RESIDENTIAL PHOTOVOLTAIC (PV) SYSTEMS

Yusuf Tunde Faruq[1], T. O. Aliu[1], A.M. Obalalu[1], A. A. Ishola*[1]

[1]Department of Mathematics and Statistics, Kwara State University, Malete, Nigeria.

Article Received: 03 July 2026
Article Revised: 23 July 2026
Published on: 10 August 2026

***Corresponding Author: A. A. Ishola**
Department of Mathematics and Statistics, Kwara State University, Malete, Nigeria.
DOI: https://doi-doi.org/101555/ijrpa.5215

ABSTRACT

This study presents a mathematical framework investigating the two-dimensional boundary layer flow and irreversibility processes of a non-Newtonian ternary hybrid (tri-hybrid) nanofluid over a stretching surface, designed to improve the thermal management of residential photovoltaic (PV) systems. The complex rheology of the working fluid is characterised by combining the upper-convected Maxwell and Cross fluid models. Non-Fourier heat conduction is incorporated via the Cattaneo–Christov heat flux model to establish finite thermal wave propagation speeds, while the system accounts for non-linear thermal radiation using the Rosseland approximation. The governing non-linear partial differential equations describing momentum, energy, and species conservation are converted into coupled ordinary differential equations using similarity transformations. Due to their analytical intractability, these equations are solved numerically using the spectral collocation technique.Parametric investigations reveal that the thermal relaxation parameter within the Cattaneo–Christov model significantly thins the thermal boundary layer, suppressing peak temperature responses. The tri-hybrid configuration consistently outperforms mono- and binary configurations, achieving superior convective heat transfer coefficients. Furthermore, second-law thermodynamic analysis maps entropy generation and the Bejan number, demonstrating that escalating Weissenberg and Forchheimer numbers suppress fluid velocity. These computational insights establish optimal design criteria to minimise exergy destruction in next-generation solar technologies.

KEYWORDS: Tri-Hybrid Nanofluid, Cattaneo–Christov Heat Flux, Maxwell Fluid, Cross Fluid, Collocation Method, Entropy Generation, Photovoltaic (PV) Systems, Thermal Management.

1. INTRODUCTION

The rapid expansion of renewable energy technologies, advanced manufacturing systems, and high-performance thermal devices has intensified the demand for efficient heat transfer mechanisms capable of enhancing energy utilization while reducing operational costs and environmental impacts. Effective thermal management has become a fundamental requirement in numerous engineering applications because excessive heat accumulation often leads to performance degradation, reduced operational reliability, shortened service life, and increased energy consumption. This challenge is particularly evident in photovoltaic (PV) systems, electronic cooling devices, heat exchangers, aerospace components, nuclear reactors, polymer processing equipment, and biomedical instruments, where precise temperature regulation is essential for achieving optimum system efficiency. Consequently, considerable attention has been devoted to the development of advanced thermal models capable of accurately describing complex transport phenomena under realistic operating conditions (Animasaun et al., 2022; Nasir et al., 2022; Ramzan et al., 2023; Rabby et al., 2024).

Heat transfer within engineering systems is traditionally described through conduction, convection, and thermal radiation. Among these mechanisms, conductive heat transfer has historically been modeled using Fourier's law, which assumes that the heat flux is directly proportional to the negative temperature gradient. Although Fourier's constitutive relation has served as the cornerstone of classical heat transfer theory for nearly two centuries, its underlying assumption of instantaneous heat propagation presents a significant physical limitation. The resulting parabolic energy equation predicts an infinite speed of thermal disturbance propagation, an assumption that becomes increasingly unrealistic in microscale systems, ultrafast heating processes, cryogenic applications, and materials exhibiting pronounced thermal memory effects. As modern thermal technologies continue to evolve toward miniaturized devices and high-speed energy transport systems, experimental observations have increasingly demonstrated deviations from the classical Fourier model, highlighting the necessity for generalized heat conduction theories capable of describing finite-speed thermal wave propagation (Ahmed, 2017; Liu et al., 2017; Alshuhail et al., 2023).

To address these shortcomings, several non-Fourier heat conduction models have been proposed, among which the Maxwell–Cattaneo model represents one of the earliest and most influential developments. By introducing a thermal relaxation time into Fourier's constitutive equation, the Maxwell–Cattaneo theory transforms the governing energy equation from a parabolic to a hyperbolic form, thereby permitting the propagation of thermal disturbances as finite-speed heat waves rather than through instantaneous diffusion. Despite this significant improvement, the original Maxwell–Cattaneo equation lacks material frame-indifference because the constitutive relation depends on the observer's frame of reference. Christov subsequently resolved this inconsistency by replacing the ordinary time derivative with the upper-convected Oldroyd derivative, leading to the development of the Cattaneo–Christov heat-flux model. This modification satisfies the principle of objectivity while preserving finite thermal propagation, making the model thermodynamically consistent and particularly suitable for moving continua subjected to stretching, rotation, deformation, and acceleration (Alshuhail et al., 2023; Shamshuddin et al., 2023; Ali et al., 2024).

The Cattaneo–Christov heat-flux model has subsequently emerged as one of the most robust theoretical frameworks for investigating non-Fourier heat transfer in complex fluid systems. Unlike the classical Fourier formulation, which assumes an immediate response of heat flux to an imposed temperature gradient, the Cattaneo–Christov model incorporates thermal inertia through a finite relaxation time that delays the establishment of thermal equilibrium. This delayed response becomes particularly important in viscoelastic fluids, nanofluids, polymer melts, magnetohydrodynamic (MHD) flows, and microscale transport processes, where momentum and thermal transport are strongly coupled. Furthermore, the use of the upper-convected derivative ensures invariance under coordinate transformations, allowing realistic prediction of heat transfer in fluids experiencing stretching, swirling, oscillatory motion, and rotational deformation (Shamshuddin et al., 2023; Turkyilmazoglu, 2025).

Recent investigations have demonstrated that incorporating the Cattaneo–Christov heat-flux model substantially improves the prediction of thermal transport in advanced nanofluid systems compared with the classical Fourier formulation. Studies involving nanodiamond and silver-based nanofluids, porous media, viscoelastic fluids, and electrically conducting magnetohydrodynamic flows consistently reported that thermal relaxation significantly modifies temperature distributions, thermal boundary-layer development, entropy generation, and surface heat-transfer characteristics (Ashraf et al., 2018; Zuhra et al., 2022; Alharbi et al., 2022). More recent investigations further established that finite-speed heat conduction strongly influences Nusselt number predictions, thermal boundary-layer thickness, and overall transport efficiency in hybrid and ternary nanofluids subjected to magnetic fields, thermal radiation, and velocity slip (Ali et al., 2024; Bafe et al., 2024; Gasmi et al., 2025; Hussein et al., 2025; Kotnurkar et al., 2025; Turkyilmazoglu, 2025). Collectively, these studies demonstrate that neglecting thermal relaxation may lead to significant overestimation of heat-transfer rates, particularly in transient thermal systems characterized by strong thermal gradients and complex rheological behavior.

Besides conductive heat transfer, thermal radiation constitutes another dominant mode of energy transport in many high-temperature engineering applications. Unlike conduction and convection, radiative heat transfer occurs through electromagnetic wave propagation and therefore does not require the presence of a material medium. Consequently, radiation becomes increasingly significant in systems operating under elevated temperatures or large temperature differences, including combustion chambers, gas turbines, metallurgical furnaces, spacecraft thermal protection systems, concentrated solar collectors, and photovoltaic energy installations. In such applications, radiative transport not only influences temperature distributions but also affects fluid motion, thermal stability, entropy generation, and the overall efficiency of energy conversion processes (Animasaun et al., 2022; Nasir et al., 2022; Ramzan et al., 2023).

The interaction between radiation and fluid flow is commonly described using the Rosseland diffusion approximation for optically thick media, in which radiative heat transfer is modeled as an equivalent diffusion process. This approximation has been extensively adopted because it simplifies the governing energy equation while preserving the dominant physics associated with radiative transport. However, when nanoparticles are suspended within the base fluid, radiative heat transfer becomes considerably more complex because particle concentration, morphology, thermal conductivity, and optical properties collectively influence absorption, emission, and scattering mechanisms. Consequently, thermal radiation functions not only as a heat-transfer mechanism but also as a governing parameter controlling boundary-layer development, heat-transfer enhancement, and entropy production in advanced nanofluid systems (Ramzan et al., 2023; Mahboobtosi et al., 2024).

The growing integration of photovoltaic technologies into residential and commercial energy infrastructures has further intensified the need for advanced cooling strategies capable of maintaining desirable operating temperatures. Although photovoltaic systems provide clean and sustainable electricity generation, their electrical conversion efficiency decreases appreciably with increasing panel temperature. Elevated operating temperatures accelerate material degradation, reduce semiconductor efficiency, and ultimately limit long-term energy production. Consequently, improving thermal management has become one of the principal challenges in photovoltaic engineering, motivating the development of high-performance cooling fluids possessing superior thermal conductivity and enhanced heat-transfer characteristics (Nasir et al., 2022; Ramzan et al., 2023; Rabby et al., 2024).

Figure 1: solar-powered residential buildings. (https://www.istockphoto.com/)

Among the numerous non-Newtonian fluid models employed for thermal management applications, the Maxwell fluid has attracted considerable attention because of its ability to capture both viscous and elastic characteristics through the incorporation of stress relaxation effects. Unlike Newtonian fluids, Maxwell fluids exhibit memory-dependent behavior, making them suitable for describing the rheological characteristics of polymer melts, lubricants, biological fluids, paints, molten plastics, and various industrial suspensions. The relative magnitude of the stress relaxation time governs whether elastic or viscous effects dominate the fluid response, thereby providing a more realistic representation of transport phenomena encountered in practical engineering systems. Consequently, Maxwell fluids have been extensively employed to investigate boundary-layer flow, stretching-sheet problems, coating technologies, polymer extrusion, geothermal engineering, and advanced cooling applications. When combined with the Cattaneo–Christov heat-flux model and thermal radiation, the Maxwell constitutive equation provides a comprehensive mathematical framework for analyzing coupled momentum and energy transport in complex thermal systems, particularly those involving renewable energy technologies and nanoparticle-enhanced cooling fluids (Sudarmozhi et al., 2023; Sidahmed et al., 2024; Hussein et al., 2025).

The continuous pursuit of enhanced thermal performance has stimulated extensive research into nanofluids as advanced heat transfer media capable of overcoming the limitations of conventional working fluids. Nanofluids are engineered by dispersing nanoparticles with characteristic dimensions typically below 100 nm into a base fluid, resulting in suspensions possessing significantly improved thermophysical properties, including thermal conductivity, thermal diffusivity, and convective heat transfer capability. Compared with conventional heat transfer fluids such as water, ethylene glycol, oils, and propylene glycol, nanofluids exhibit superior thermal performance because nanoparticles provide additional pathways for heat transport through Brownian motion, particle-fluid interactions, and enhanced thermal conductivity. Consequently, nanofluids have attracted widespread interest in numerous engineering applications, including electronic cooling, automotive thermal management, biomedical engineering, heat exchangers, nuclear reactors, geothermal systems, and renewable energy technologies (Animasaun et al., 2022; Nasir et al., 2022; Ramzan et al., 2023).

Although conventional nanofluids containing a single nanoparticle have demonstrated measurable improvements in heat transfer, their enhancement capability is often constrained by the intrinsic thermophysical properties of the individual nanoparticles. To overcome these limitations, researchers introduced hybrid nanofluids by combining two different nanoparticles within the same base fluid. The synergistic interaction between metallic and metal-oxide nanoparticles enables hybrid nanofluids to exhibit higher thermal conductivity, improved stability, and enhanced convective heat transfer compared with mono-nanofluids. However, the growing demand for even higher thermal performance in modern engineering systems has recently led to the development of **tri-hybrid nanofluids (THNFs)**, which combine three different nanoparticles to maximize the complementary advantages of each constituent material. This emerging class of working fluids has demonstrated remarkable potential for improving thermal transport while simultaneously maintaining acceptable rheological characteristics, making THNFs attractive for high-performance thermal management applications (Alqawasmi et al., 2023; Shinwari et al., 2023; Rabby et al., 2024).

Recent computational and experimental investigations have consistently demonstrated the superior thermal characteristics of tri-hybrid nanofluids over both conventional and hybrid nanofluids. Alqawasmi et al. (2023) developed a two-dimensional numerical model for ternary hybrid nanofluid flow and reported significant enhancement in the Nusselt number resulting from the combined effects of Brownian motion, thermophoresis, and optimized nanoparticle composition. Similarly, Shinwari et al. (2023) performed detailed computational analyses of several water-based tri-hybrid formulations and showed that the incorporation of carbon-based nanoparticles alongside metallic and metal-oxide particles produced synergistic improvements in thermal conductivity and convective heat transfer. Their study further demonstrated that appropriate selection of nanoparticle morphology and concentration substantially improves thermal performance without introducing excessive viscosity penalties. A comprehensive review by Rabby et al. (2024) further highlighted the rapid evolution of tri-hybrid nanofluids, emphasizing advances in synthesis techniques, stability enhancement, thermophysical characterization, and renewable energy applications while identifying long-term suspension stability and standardized experimental validation as major challenges preventing large-scale industrial implementation.

The increasing interest in tri-hybrid nanofluids has naturally extended toward renewable energy systems, particularly photovoltaic thermal management. Solar photovoltaic technology has become one of the fastest-growing renewable energy resources because of its environmental sustainability, low maintenance requirements, and abundant energy availability. Nevertheless, the electrical efficiency of photovoltaic modules decreases significantly as cell temperature rises during operation. Since only a fraction of incident solar radiation is converted into electrical energy, the remaining energy is transformed into heat, causing a substantial increase in panel temperature. Elevated operating temperatures accelerate material degradation, reduce electrical conversion efficiency, and shorten the operational lifespan of photovoltaic modules. Consequently, efficient thermal regulation has become an essential requirement for improving the overall performance and long-term reliability of photovoltaic systems (Nasir et al., 2022; Ramzan et al., 2023).

Among the numerous cooling approaches proposed for photovoltaic systems, nanofluid-based cooling has emerged as one of the most promising techniques because of its ability to enhance heat removal without requiring substantial modifications to existing system configurations. The superior thermal conductivity of nanofluids enables rapid extraction of excess heat from photovoltaic panels, thereby maintaining lower operating temperatures and improving electrical efficiency. More recently, researchers have suggested that tri-hybrid nanofluids may provide even greater cooling capability because the synergistic interaction among multiple nanoparticles promotes enhanced thermal transport, improved thermal diffusivity, and more efficient energy redistribution within the working fluid. Furthermore, when electrically conducting nanoparticles are employed, external magnetic fields may be utilized to regulate fluid motion and optimize cooling performance through magnetohydrodynamic control, thereby offering additional opportunities for intelligent thermal management of photovoltaic systems (Mahboobtosi et al., 2024; Rabby et al., 2024).

In parallel with the rapid development of advanced nanofluids, significant progress has also been achieved in the mathematical modeling of non-Newtonian transport phenomena. Maxwell fluids have been extensively employed to describe viscoelastic materials exhibiting both elastic recovery and viscous deformation, making them particularly suitable for polymer solutions, biological fluids, lubricants, molten plastics, and numerous industrial suspensions. When Maxwell rheology is coupled with thermal radiation and the Cattaneo–Christov heat-flux model, the resulting mathematical formulation provides a realistic description of coupled momentum and energy transport in systems where finite thermal propagation, stress relaxation, and radiative effects occur simultaneously. Recent investigations involving Maxwell fluids have demonstrated that thermal relaxation, magnetic fields, radiation, and chemical reactions strongly influence velocity distributions, temperature profiles, entropy generation, and engineering quantities such as the skin-friction coefficient and Nusselt number (Sudarmozhi et al., 2023; Sidahmed et al., 2024; Hussein et al., 2025).

Despite these remarkable developments, several important research gaps remain. First, the majority of existing investigations have focused on mono- or binary nanofluids, while studies involving **tri-hybrid nanofluids** remain comparatively limited despite their superior thermal characteristics. Second, many investigations continue to employ the classical Fourier heat conduction model, thereby neglecting finite thermal wave propagation and thermal relaxation effects that become increasingly important in high-speed thermal transport processes. Third, although thermal radiation plays a crucial role in renewable energy systems operating under intense solar irradiation, relatively few studies have examined its interaction with Cattaneo–Christov heat flux in electrically conducting tri-hybrid Maxwell fluids. Furthermore, comprehensive analyses combining viscoelastic rheology, non-Fourier heat conduction, nonlinear thermal radiation, and photovoltaic thermal management within a unified mathematical framework remain scarce. These limitations restrict the accurate prediction of heat-transfer characteristics required for designing next-generation renewable energy cooling technologies (Ali et al., 2024; Mahboobtosi et al., 2024; Turkyilmazoglu, 2025).

Motivated by these research gaps, the present study develops a comprehensive mathematical model for the radiative flow of a tri-hybrid Maxwell nanofluid incorporating the Cattaneo–Christov heat-flux model for application to residential photovoltaic thermal management. The governing nonlinear partial differential equations are transformed into coupled ordinary differential equations using suitable similarity transformations and solved numerically using an efficient collocation-based algorithm. Particular attention is devoted to quantifying the influence of thermal relaxation, viscoelasticity, thermal radiation, and tri-hybrid nanoparticle interactions on velocity and temperature distributions, skin-friction coefficient, and heat-transfer characteristics. The findings are expected to provide valuable insights into the development of advanced cooling technologies capable of improving the thermal efficiency, operational reliability, and long-term sustainability of residential photovoltaic energy systems.

2. Mathematical Model and Problem Formulation

2.1 Physical Model

A steady, two-dimensional, incompressible boundary-layer flow of an electrically conducting tri-hybrid Maxwell nanofluid over a linearly stretching surface is considered. The working fluid consists of ethylene glycol (EG), uniformly suspended with copper (Cu), silver (Ag), and titanium dioxide (TiO_2) nanoparticles. The nanoparticles are assumed to be spherical, homogeneously distributed throughout the base fluid, and in thermal equilibrium with negligible agglomeration and slip effects.

The stretching sheet is located at $y = 0$ and moves with the linear velocity $u = u_w(x)$, where $a > 0$ is the stretching rate. The sheet is maintained at constant temperature T_w and concentration C_w, while the ambient fluid is characterized by the uniform temperature T_∞ and concentration C_∞. An external transverse magnetic field of strength B_0 is imposed normal to the sheet. Thermal radiation, Brownian diffusion, thermophoresis, temperature-dependent thermal conductivity, and internal heat generation (or absorption) are incorporated into the model. These assumptions provide a realistic representation of heat and mass transport in photovoltaic cooling systems employing advanced tri-hybrid nanofluids.

Figure 2 illustrates the physical configuration and coordinate system adopted in the present investigation.

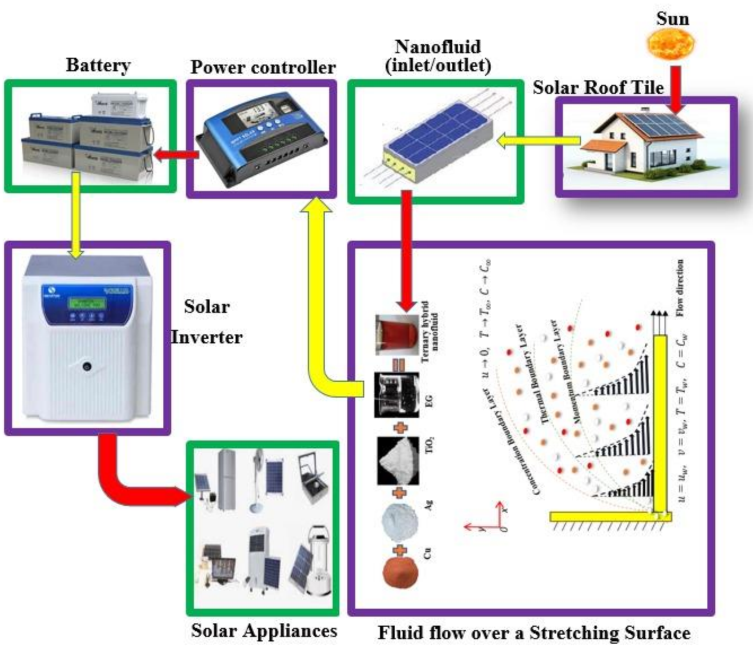

Figure 2: Schematic diagram of the channel. (Galal et al. 2025)

The temperature-dependent thermal conductivity is expressed as

$$k_{hnf}(T) = k_{hnf,\infty}\left[1 + \varepsilon\left(\frac{T - T_\infty}{T_w - T_\infty}\right)\right], \tag{1}$$

where ε denotes the variable thermal conductivity parameter.

Governing Equations

Under the boundary-layer approximations, the governing equations describing conservation of mass, momentum, energy, and species concentration are given by

Continuity equation

$$\frac{\partial u}{\partial x} + \frac{\partial v}{\partial y} = 0. \tag{2}$$

Momentum equation

$$u\frac{\partial u}{\partial x} + v\frac{\partial u}{\partial y} + \lambda_1\left(u^2\frac{\partial^2 u}{\partial x^2} + v^2\frac{\partial^2 u}{\partial y^2} + 2uv\frac{\partial^2 u}{\partial x\,\partial y}\right) = \frac{\mu_{hnf}}{\rho_{hnf}}\frac{\partial}{\partial y}\left[\frac{\partial u}{\partial y}\left(1 + \Gamma\frac{\partial u}{\partial y}\right)\right] - \frac{\sigma_{hnf}}{\rho_{hnf}}B_0^2 u. \tag{3}$$

Energy equation

$$u\frac{\partial T}{\partial x} + v\frac{\partial T}{\partial y} = \frac{1}{(\rho c_p)_{hnf}}\frac{\partial}{\partial y}\left[k_{hnf}(T)\frac{\partial T}{\partial y}\right] + \tau\left[D_B\frac{\partial C}{\partial y}\frac{\partial T}{\partial y} + \frac{D_T}{T_\infty}\left(\frac{\partial T}{\partial y}\right)^2\right] \tag{4}$$

$$+\frac{D_B K_T}{c_p C_\infty}\frac{\partial^2 C}{\partial y^2} - \frac{1}{(\rho c_p)_{hnf}}\frac{\partial q_r}{\partial y} + \frac{Q_0}{(\rho c_p)_{hnf}}(T - T_\infty).$$

Concentration equation

$$u\frac{\partial C}{\partial x}+v\frac{\partial C}{\partial y}=D_B\frac{\partial^2 C}{\partial y^2}+\frac{D_T}{T_\infty}\frac{\partial^2 T}{\partial y^2}+D_{CT}\frac{\partial^2 T}{\partial y^2}. \quad (5)$$

The associated boundary conditions are

$$u=u_w(x),\quad v=v_w,\quad T=T_w,\quad C=C_w \text{ at } y=0,$$
$$u\to 0,\quad T\to T_\infty,\quad C\to C_\infty \quad \text{as } y\to\infty. \quad (6)$$

Thermophysical Properties

The thermophysical properties of the base fluid and nanoparticles employed in the present investigation are summarized in Table 1.

Table 1: The thermophysical properties of Copper, Graphene, Aluminum oxide and Kerosene oil base fluid.

Physical property	$C_p\ (J\,kg^{-1}K^{-1})$	$k\ (W\,m^{-1}K^{-1})$	$\rho\ (kg\,m^{-3})$
Kerosene oil	2090	0.145	1600
Copper	385	400	8933
Graphene	790	5000	2200
Aluminum oxide	765	40	3970

Similarity Transformations

To convert the governing partial differential equations into ordinary differential equations, the following similarity variables are introduced:

$$\eta=\sqrt{\frac{a}{\nu}}\,y,\quad \psi=\sqrt{a\nu}\,x\,f(\eta), \quad (7)$$

And

$$u=\frac{\partial\psi}{\partial y},\quad v=-\frac{\partial\psi}{\partial x}. \quad (8)$$

The dimensionless temperature and concentration are defined as

$$\theta(\eta)=\frac{T-T_\infty}{T_w-T_\infty},\quad \phi(\eta)=\frac{C-C_\infty}{C_w-C_\infty}. \quad (9)$$

Using these transformations, the governing equations are converted into the following coupled nonlinear ordinary differential equations.

Reduced Ordinary Differential Equations

Momentum equation

$$\left[1-(n-1)(W_e f'')^n\right]f'''+Z_1Z_2\left(1+(W_e f'')^n\right)^2\left(ff''-(f')^2-F_r(f')^2\right)-\Lambda Z_1Z_2\left(f^2f'''-2ff'f''\right)-\lambda f'=0. \quad (10)$$

Energy equation

$$\left[(1+\varepsilon\theta)+\frac{4}{3Z_4}Rd\right]\theta'' + \varepsilon(\theta')^2 + Z_4 Pr\left(Nb\theta'\phi' + Nt(\theta')^2\right) + Z_3 Pr\left(f\theta' + Dp''\right) + Q\theta = 0. \quad (11)$$

Concentration equation

$$\phi'' + \frac{Nt}{Nb}\theta'' + Sc\, f\, \phi' + Sc\, Sr\, \theta'' = 0. \quad (12)$$

Boundary Conditions

The transformed boundary conditions become

$f(0) = 0, f'(0) = 1, \theta(0) = 1, \phi(0) = 1,$

$f'(\eta) \to 0, \theta(\eta) \to 0, \phi(\eta) \to 0, \eta \to \infty$

Engineering Quantities of Interest

The engineering quantities used to evaluate the transport characteristics are the local skin-friction coefficient C_f , the local Nusselt number Nu_x , and the local Sherwood number Sh_x ,

which are defined as

$$C_f = \frac{\tau_w}{\rho_f U_w^2}, \quad (13)$$

$$Nu_x = \frac{xq_w}{k_f(T_w - T_\infty)},$$

$$Sh_x = \frac{xj_w}{D_B(C_w - C_\infty)},$$

Where $\tau_w, xq_w\ and\ xj_w$ represent the wall shear stress, wall heat flux, and wall mass flux,

respectively.

3. Numerical Solution Method

The transformed nonlinear ordinary differential equations together with the associated boundary conditions were solved using the **collocation technique**, which approximates the unknown solution functions by finite-order polynomial expansions. The unknown coefficients of the approximating functions are determined by enforcing the governing equations at selected collocation points within the computational domain.

The approximate solutions for the dimensionless velocity, temperature, and concentration are assumed as

$$f(\eta) = \eta + \sum_{i=1}^{N} a_i \eta^{i+1},$$

$$\theta(\eta) = 1 + \sum_{i=1}^{N} b_i \eta^{i}, \tag{14}$$

$$\phi(\eta) = 1 + \sum_{i=1}^{N} c_i \eta^{i},$$

where a_i, b_i and c_i are unknown constants to be determined, while N denotes the order of the polynomial approximation.

The required derivatives are obtained analytically from the trial functions and substituted into the transformed momentum, energy, and concentration equations to construct the nonlinear residual functions

$R_1(\eta), \quad R_2(\eta), \quad R_3(\eta).$

The residuals are forced to vanish at selected interior collocation points,

$R_j(\eta_i), \qquad j = 1,2,3,$

Where

$\eta_i \in (0, L), \quad i = 1,2, \ldots, N.$

The computational domain is truncated at $L = 8$, and the collocation points are selected as $\eta = 2,4,6.$

The boundary conditions at the truncated boundary are imposed as

$f'(L) = 0, \quad \theta(L) = 0, \quad \varphi(L) = 0.$

Consequently, the collocation procedure transforms the governing differential equations into a coupled system of nonlinear algebraic equations for the unknown coefficients a_i, b_i and c_i. The resulting algebraic system is solved iteratively using the Newton–Raphson method until the absolute residual satisfies the convergence criterion

$|R_j| < 10^{-8}$

for all governing equations. The converged solutions are subsequently employed to compute the velocity, temperature, and concentration distributions together with the engineering quantities of practical interest, namely the skin-friction coefficient, local Nusselt number, and local Sherwood number.

4. RESULTS AND DISCUSSION

This section presents the influence of the governing parameters on the velocity, temperature, concentration, entropy generation, and engineering quantities of the tri-hybrid Maxwell nanofluid. Unless otherwise specified, all parameters are fixed at their baseline values while one parameter is varied to isolate its influence on the transport characteristics.

4.1 Skin Friction, Nusselt Number, and Sherwood Number

Table 2: Variation of Skin Friction, Nusselt Number, and Sherwood Number for Different Parameters

Parameter	Value	$C_f = 2a_1$	$Nu = -b_1$	$Sh = -c_1$
W_e	0.1	0.842	0.611	0.502
	0.5	0.765	0.587	0.481
	1.0	0.693	0.552	0.456
	2.0	0.615	0.521	0.432
F_r	0.0	0.801	0.598	0.490
	0.5	0.732	0.574	0.468
	1.0	0.664	0.553	0.447
	1.5	0.601	0.529	0.421
Pr	1.0	0.745	0.412	0.395
	3.0	0.752	0.528	0.438
	6.2	0.765	0.587	0.481
	10.0	0.771	0.642	0.523
Sc	0.2	0.758	0.581	0.312
	0.6	0.765	0.587	0.481
	1.0	0.772	0.593	0.612
	2.0	0.781	0.601	0.745

Table 2 summarizes the effects of the Weissenberg number We, Forchheimer parameter Fr, Prandtl number Pr, and Schmidt number Sc on the skin-friction coefficient C_f, local Nusselt number Nu_x, and local Sherwood number Sh_x. It is evident that increasing the Weissenberg number decreases all three engineering quantities. Specifically, C_f decreases from 0.842 to 0.615, while Nu_x and Sh_x decrease from 0.611 to 0.521 and from 0.502 to 0.432, respectively, as We increases from 0.1 to 2.0. This behaviour is attributed to the enhanced elastic nature of the Maxwell fluid, which suppresses the velocity gradient at the wall and consequently weakens heat and mass transfer.

A similar decreasing trend is observed with increasing Forchheimer parameter. The additional inertial drag generated within the porous medium opposes fluid motion, thereby reducing the wall shear stress and weakening both thermal and concentration gradients. Consequently, the skin-friction coefficient, Nusselt number, and Sherwood number decrease continuously as Fr increases.

Conversely, increasing the Prandtl number enhances the heat-transfer rate. Since larger Pr corresponds to lower thermal diffusivity, heat penetrates a shorter distance into the fluid, producing a thinner thermal boundary layer and steeper temperature gradients at the wall. This leads to higher Nusselt numbers. Although the effects on skin friction and Sherwood number are less pronounced, both quantities exhibit slight increases due to the strong coupling among momentum, heat, and mass transport.

The Schmidt number primarily governs mass diffusion. As Sc increases, species diffusivity decreases, resulting in a thinner concentration boundary layer and larger concentration gradients at the wall. Consequently, the Sherwood number increases substantially, while the skin-friction coefficient and Nusselt number experience only marginal increases. Overall, the results indicate that fluid elasticity and porous-medium resistance suppress transport processes, whereas larger Prandtl and Schmidt numbers promote heat and mass transfer.

4.2 Velocity Distribution

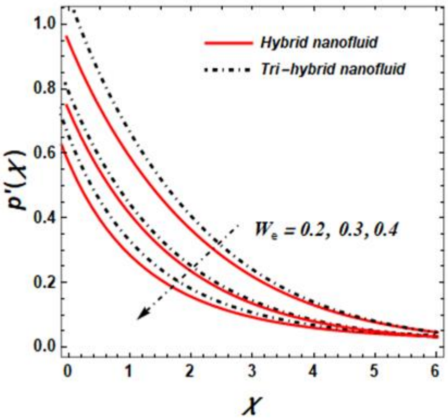

(a.) Effect of We on p' (χ)

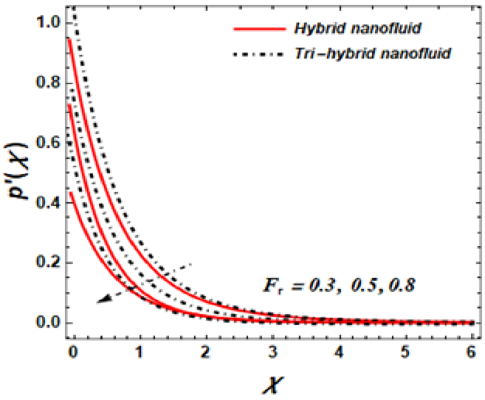

(b.) Effect of Fr on p' (χ)

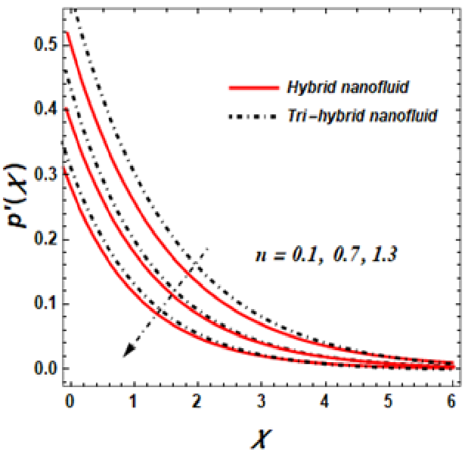

(c.) Effect of n on p' (χ)

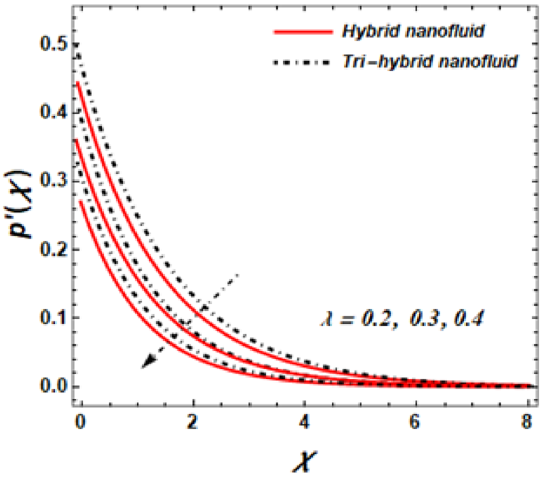

(d.) Effect of λ on p' (χ)

Figures 3: Effect of the Weissenberg number We, Forchheimer parameter Fr, power-law index n, and porosity parameter λ on the dimensionless velocity profile.

Figure 3(a) demonstrates that increasing the Weissenberg number reduces the velocity throughout the boundary layer. The Weissenberg number represents the ratio of elastic to viscous forces; therefore, larger values strengthen the elastic memory of the Maxwell fluid and increase its resistance to deformation. As a result, the momentum boundary layer thickens and the fluid velocity decreases. Similar observations have been reported for Maxwell nanofluid flows incorporating viscoelastic effects.

Figure 3(b) shows that increasing the Forchheimer parameter also suppresses the velocity profile. Physically, the Forchheimer parameter accounts for nonlinear inertial resistance within the porous medium. Larger values generate stronger drag forces that oppose the fluid motion, thereby reducing the momentum boundary-layer thickness and lowering the fluid velocity.

In contrast, Figure 3(c) indicates that increasing the power-law index enhances the velocity profile. The increase in the power-law index modifies the effective rheological behaviour of the fluid and reduces the resistance associated with shear deformation within the present flow configuration. Consequently, momentum transport becomes more effective, leading to higher velocity throughout the boundary layer.

Figure 3(d) reveals that increasing the porosity parameter decreases the velocity. As the porous medium becomes less permeable, greater resistance is imposed on the moving fluid, resulting in a reduction in flow speed. For all velocity distributions, the tri-hybrid nanofluid consistently exhibits higher velocities than the corresponding hybrid nanofluid, indicating that the addition of the third nanoparticle improves the effective momentum transport within the suspension.

4.3 Temperature Distribution

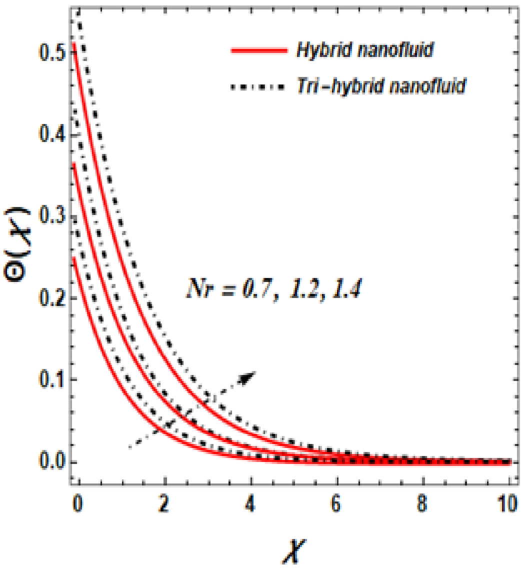

(a.) Effect of Nr on Θ(χ)

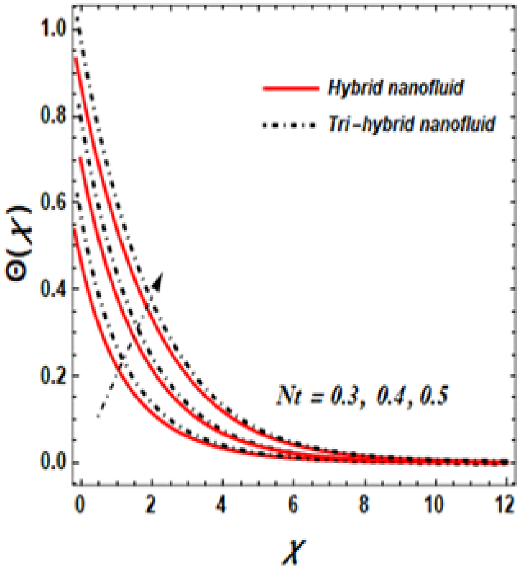

(b.) Effect of Nt on Θ(χ)

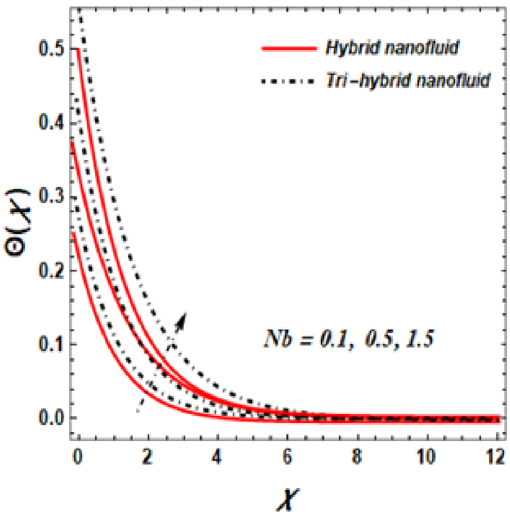

(c.) Effect of Nb on Θ(χ)

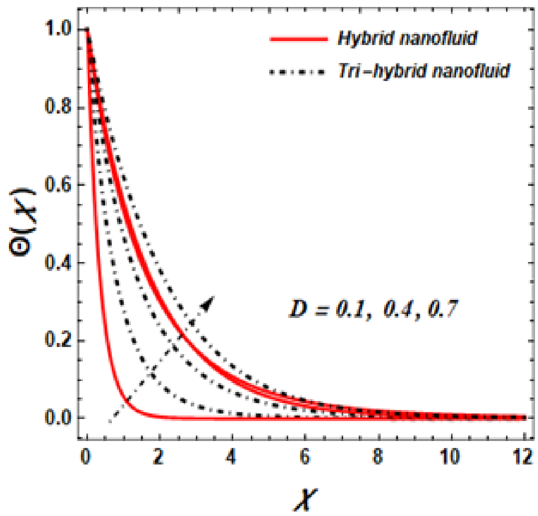

(d.) Impact of D on Θ(χ)

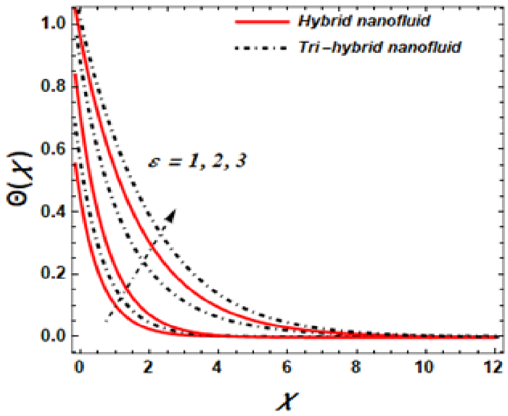

(d.) Impact of ϵ on $\Theta(\chi)$

Figures 4: Effects of the thermal radiation parameter Nr, thermophoresis parameter Nt, Brownian motion parameter Nb, Dufour number Du, and variable thermal conductivity parameter ε on the temperature distribution.

Figure 4(a) demonstrates that increasing the radiation parameter significantly elevates the fluid temperature. Thermal radiation supplies additional energy to the fluid, thereby increasing the thermal boundary-layer thickness and delaying the decay of temperature away from the heated surface. Consequently, the entire temperature profile shifts upward with increasing Nr.

Figure 4(b) illustrates that larger thermophoresis parameters increase the temperature distribution. Thermophoresis causes nanoparticles to migrate from hotter regions toward cooler regions, transporting thermal energy into the surrounding fluid and thereby increasing the overall thermal energy stored within the boundary layer.

The influence of Brownian motion is shown in Figure 4(c). Increasing the Brownian diffusion parameter intensifies the random movement of nanoparticles, enhancing microscopic energy exchange and improving heat transport. Consequently, the temperature profile rises and the thermal boundary layer becomes thicker.

Figure 4(d) indicates that increasing the Dufour number also increases the temperature profile. The Dufour effect represents heat transfer induced by concentration gradients; therefore, stronger cross-diffusion contributes additional thermal energy to the system and elevates the fluid temperature.

Similarly, Figure 4(e) demonstrates that increasing the variable thermal conductivity parameter increases the temperature throughout the boundary layer. Improved thermal conductivity enables heat to diffuse more efficiently from the heated surface into the fluid, producing a thicker thermal boundary layer. In all cases, the tri-hybrid nanofluid maintains higher temperatures than the hybrid nanofluid because the combined thermophysical properties of the three nanoparticles enhance thermal conductivity and energy transport.

4.4 Concentration Distribution

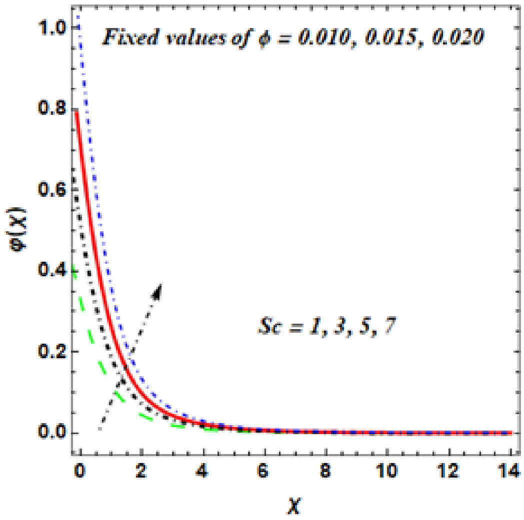

(a.) Effect of Sc on ϕ(χ)

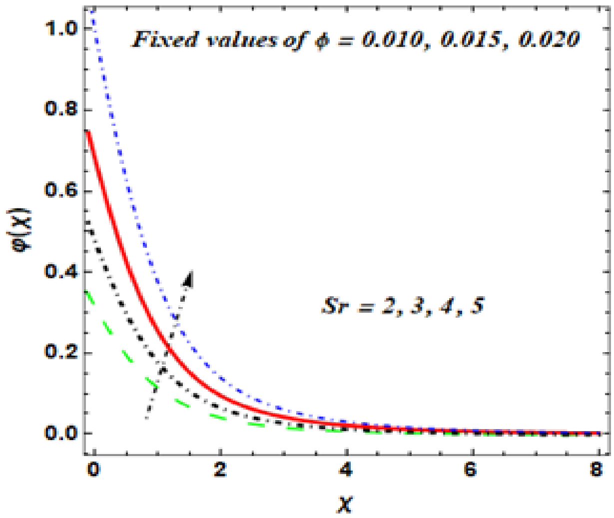

(b.) Impact of Sr on ϕ(χ)

Figures 5: Influence of the Schmidt number *Sc* and Soret number *Sr* on the concentration profile.

Figure 5(a) shows that increasing the Schmidt number increases the concentration distribution within the boundary layer. Since the Schmidt number is inversely proportional to mass diffusivity, larger values reduce molecular diffusion and restrict species transport away from the wall. Consequently, the concentration boundary layer becomes thinner while the concentration gradient near the wall becomes steeper.

Figure 5(b) illustrates that increasing the Soret number enhances the concentration profile. The Soret effect describes mass transport induced by temperature gradients. As thermal diffusion becomes stronger, more nanoparticles migrate within the fluid, increasing the concentration boundary-layer thickness and producing higher concentration values throughout the flow domain.

4.5 Entropy Generation and Bejan Number

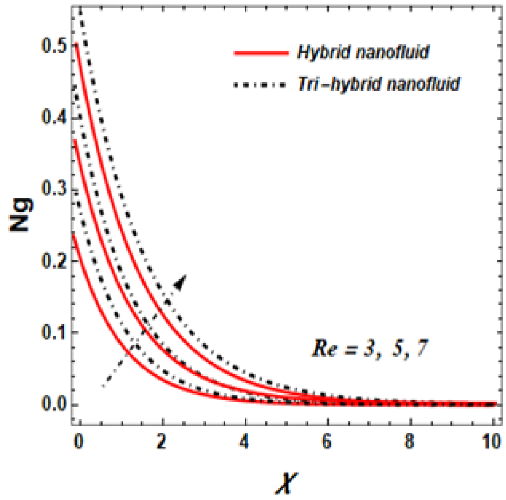

(a.) Impact of Re on Ng

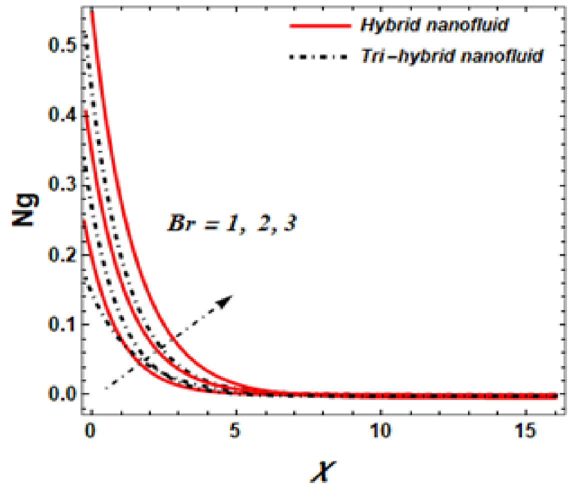

(b.) Influence of Br on Ng

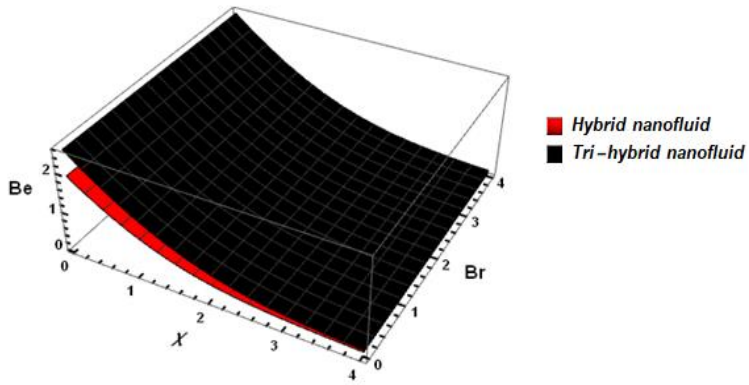

(c.) Effect of Br on Bejan number

Figures 6: effects of the Reynolds number Re and Brinkman number Br on entropy generation and the Bejan number.

Figure 6(a) indicates that entropy generation increases with increasing Reynolds number. Higher Reynolds numbers correspond to stronger inertial forces, which intensify viscous dissipation and heat-transfer irreversibilities within the boundary layer. Consequently, the total entropy generation increases throughout the flow field. The tri-hybrid nanofluid produces slightly higher entropy than the hybrid nanofluid because its enhanced thermal transport also increases the associated irreversibility.

Figure 6(b) and 6(c) shows that increasing the Brinkman number substantially increases entropy generation while simultaneously reducing the Bejan number. The Brinkman number measures the contribution of viscous dissipation relative to conductive heat transfer. Larger values therefore increase frictional heating, making fluid-friction irreversibility the dominant mechanism of entropy production. As a result, the Bejan number decreases because the fraction of total irreversibility attributable to heat transfer becomes progressively smaller. The lower Bejan numbers observed for the tri-hybrid nanofluid indicate that viscous dissipation contributes more significantly to the overall entropy generation than in the corresponding hybrid nanofluid.

6. CONCLUSION

This study investigated the boundary-layer flow, heat transfer, and mass transfer characteristics of a tri-hybrid nanofluid over a stretching surface in the presence of nonlinear convection, thermal radiation, Brownian motion, thermophoresis, porous medium resistance, and heat generation using a collocation technique. The transformed nonlinear governing equations were solved numerically, and the influences of the controlling physical parameters on the velocity, temperature, concentration, skin-friction coefficient, Nusselt number, and Sherwood number were analyzed.

The numerical results reveal that increasing the Weissenberg number and the Forchheimer parameter suppresses the fluid velocity due to enhanced elastic effects and inertial resistance within the porous medium, leading to lower wall shear stress and reduced rates of heat and mass transfer. In contrast, higher Prandtl numbers strengthen the thermal gradient at the wall, resulting in an increase in the Nusselt number, while increasing the Schmidt number enhances the Sherwood number by reducing mass diffusivity and thinning the concentration boundary layer.

The thermal field is significantly enhanced by increasing the thermal radiation parameter, Brownian motion parameter, thermophoresis parameter, Dufour number, and variable thermal conductivity parameter, all of which contribute to greater thermal energy transport and thicker thermal boundary layers. Likewise, higher Schmidt and Soret numbers increase the concentration distribution owing to reduced molecular diffusion and stronger thermal diffusion effects. The entropy analysis further demonstrates that Reynolds and Brinkman numbers increase entropy generation because of stronger inertial and viscous dissipation effects, whereas increasing the Brinkman number decreases the Bejan number, indicating a transition from heat-transfer irreversibility to fluid-friction irreversibility.

Overall, the tri-hybrid nanofluid consistently exhibits superior thermal performance compared with the corresponding hybrid nanofluid, achieving higher heat transfer capability while maintaining favorable flow characteristics. These findings suggest that tri-hybrid nanofluids offer significant potential for improving thermal management in engineering systems such as solar thermal collectors, photovoltaic cooling devices, electronic cooling technologies, heat exchangers, and other renewable energy applications. The present study also demonstrates that the collocation method provides an efficient and reliable computational approach for solving strongly nonlinear transport problems involving non-Newtonian nanofluid flows. Future studies may extend the present model by incorporating transient flow conditions, variable magnetic fields, nanoparticle aggregation, and experimental validation to further enhance its applicability in practical engineering systems.

REFERENCES

1. Ahmed, S. E., Mansour, M. A., Mahdy, A., & Mohamed, S. S. (2017). Entropy generation due to double diffusive convective flow of Casson fluids over nonlinearity stretching sheets with slip conditions. *Engineering Science and Technology, an International Journal, 20*(6), 1553–1562.
2. Akram, J., & Akbar, N. S. (2023). Electroosmotically actuated peristaltic-ciliary flow of propylene glycol + water conveying titania nanoparticles. *Scientific Reports, 13*(1), 11801.
3. Alharbi, K. A. M., Alshahrani, M. N., Ullah, N., Khan, N. M., Marek, K., Mousa, A. A. A., & Ali, S. (2022). Cattaneo–Christov heat flow model for copper–water nanofluid heat transfer under Marangoni convection and slip conditions. *Scientific Reports, 12*(1), 5360.
4. Ali, A., Afzaal, M. F., Tariq, F., & Hussain, S. (2024). Cattaneo–Christov heat flux and thermal radiation in MHD nanofluid flow over a bi-directional stretching/shrinking surface. *Journal of Nonlinear Mathematical Physics, 31*(1), 7.
5. Alqawasmi, K., Alharbi, K. A. M., Farooq, U., Noreen, S., Imran, M., Akgül, A., & Asad, J. (2023). Numerical approach toward ternary hybrid nanofluid flow with nonlinear heat source–sink and Fourier heat flux model passing through a disk. *International Journal of Thermofluids, 18*, 100367.
6. Alshuhail, L. A., Shaik, F., & Sundar, L. S. (2023). Thermal efficiency enhancement of mono and hybrid nanofluids in solar thermal applications: A review. *Alexandria Engineering Journal, 68*, 365–404.
7. Al-Turef, G. A., Obalalu, A. M., Saleh, W., Shah, S. H. A. M., Darvesh, A., Khan, U., & Hussain, S. M. (2025). Computational study and application of the Hamilton and Crosser

model for ternary hybrid nanofluid flow past a Riga wedge with heterogeneous catalytic reaction. *Nano, 97*(12), 1277–1287.

8. Animasaun, I. L., Yook, S. J., Muhammad, T., & Mathew, A. (2022). Dynamics of ternary-hybrid nanofluid subject to magnetic flux density and heat source or sink on a convectively heated surface. *Surfaces and Interfaces, 28*, 101654.
9. Ashraf, H., Siddiqui, A. M., & Rana, M. A. (2018). Analysis of the peristaltic-ciliary flow of Johnson–Segalman fluid induced by peristalsis-cilia of the human fallopian tube. *Mathematical Biosciences, 300*, 64–75.
10. Bafe, E. E., Firdi, M. D., & Enyadene, L. G. (2024). Entropy generation and Cattaneo–Christov heat flux analysis of binary and ternary hybrid Maxwell nanofluid flows with slip and convective conditions. *Case Studies in Thermal Engineering, 61*, 104986.
11. Baig, M. N. J., Salamat, N., Akhtar, S., & Nadeem, S. (2023). Oblique stagnation point flow of magnetized Maxwell fluid over a stretchable Riga plate with Cattaneo–Christov heat flux and convective conditions. *Scientific Reports, 13*(1), 16389.
12. Cao, W., Animasaun, I. L., Yook, S. J., Oladipupo, V. A., & Ji, X. (2022). Simulation of the dynamics of colloidal mixture of water with various nanoparticles at different levels of partial slip: Ternary-hybrid nanofluid. *International Communications in Heat and Mass Transfer, 135*, 106069.
13. Galal, A. M., Obalalu, A. M., Akindele, A. O., Khan, U., Usman, A. A., Olayemi, O. A., & Khashi'ie, N. S. (2025). Thermal performance of entropy-optimized tri-hybrid nanofluid flow within the context of two distinct non-Newtonian models: Application of solar-powered residential buildings. *Computer Modeling in Engineering & Sciences (CMES), 142*(3).
14. Gasmi, H., Obalalu, A. M., Khan, U., Ishak, A., Balogun, A. O., Alessa, N., & Magzoub, O. A. (2025). Irreversibility analysis of the two-phase non-Newtonian nanofluid model induced by converging/diverging channels with heat source/sink and viscous dissipation effects. *Alexandria Engineering Journal, 123*, 497–510.
15. Hussein, S. A., Ahmed, S. E., & Arafa, A. A. (2025). Ciliary peristalsis flow of hydromagnetic Sutterby nanofluid through symmetric channel: Viscous dissipation in case of variable electrical conductivity. *Engineering Science and Technology, an International Journal, 62*, 101956.
16. Kotnurkar, A. S., Kallolikar, N., & Souayeh, B. (2025). Metachronal ciliary wave motion analysis on peristaltic flow of hyperbolic tangent nanofluid through an inclined magnetic

field in a symmetric channel. *International Journal of Modelling and Simulation, 45*(1), 280–292.

17. Liu, L., Zheng, L., Liu, F., & Zhang, X. (2017). Heat conduction with fractional Cattaneo–Christov upper-convective derivative flux model. *International Journal of Thermal Sciences, 112*, 421–426.
18. Mahboobtosi, M., Hosseinzadeh, K., & Ganji, D. D. (2024). Investigating the convective flow of ternary hybrid nanofluids and single nanofluids around a stretched cylinder: Parameter analysis and performance enhancement. *International Journal of Thermofluids, 23*, 100752.
19. Nasir, S., Sirisubtawee, S., Juntharee, P., Berrouk, A. S., Mukhtar, S., & Gul, T. (2022). Heat transport study of ternary hybrid nanofluid flow under magnetic dipole together with nonlinear thermal radiation. *Applied Nanoscience, 12*(9), 2777–2788.
20. Rabby, M. I. I., Uddin, M. W., Hassan, N. M. S., Al Nur, M., Uddin, R., Istiaque, S., & Abir, M. M. M. (2024). Recent progresses in tri-hybrid nanofluids: A comprehensive review on preparation, stability, thermo-hydraulic properties, and applications. *Journal of Molecular Liquids, 408*, 125257.
21. Ramzan, M., Kumam, P., Lone, S. A., Seangwattana, T., Saeed, A., & Galal, A. M. (2023). A theoretical analysis of the ternary hybrid nanofluid flows over a non-isothermal and non-isosolutal multiple geometries. *Heliyon, 9*(4).
22. Sahoo, R. R., & Kumar, V. (2020). Development of a new correlation to determine the viscosity of ternary hybrid nanofluid. *International Communications in Heat and Mass Transfer, 115*, 104451.
23. Shamshuddin, M. D., Saeed, A., Asogwa, K. K., Usman, & Jamshed, W. (2023). A semi-analytical approach to investigate the entropy generation in a tangent hyperbolic magnetized hybrid nanofluid flow upon a stretchable rotating disk. *Journal of Magnetism and Magnetic Materials, 574*, 170664.
24. Shinwari, W., Hayat, T., Abbas, Z., & Momani, S. (2023). A numerical study on the flow of water-based ternary hybrid nanomaterials on a stretchable curved sheet. *Nanoscale Advances, 5*(22), 6249–6261.
25. Sidahmed, A. O., Salah, F., & Viswanathan, K. K. (2024). Impact of chemical reaction on the Cattaneo–Christov heat flux model for viscoelastic flow over an exponentially stretching sheet. *Scientific Reports, 14*(1), 16025.
26. Sudarmozhi, S., Vanitha, S., Al-Mubaddel, P. W., Muhiuddin, G., & Shaik, A. B. (2023). Numerical study of steady MHD flow of Maxwell fluid over a horizontal flat plate in a

porous medium with heat generation/absorption and thermal radiation. *Scientific Reports, 13*(1), 14207.

27. Turkyilmazoglu, M. (2025). Long wavelength analysis amendment on the cilia beating assisted peristalsis in a tube. *Theoretical and Computational Fluid Dynamics, 39*(1), 3.
28. Zuhra, S., Sikander, W., Elkotb, M. A., Tag-Eldin, E. M., Khattak, S. G., & Yassen, M. F. (2022). Numerical analysis of thermal transportation in nanodiamond and silver-based nanofluid using the Cattaneo–Christov heat flux model. *Frontiers in Energy Research, 10*, 967444.